World Electric Vehicle Journal

Article

State-Feedback Control of Interleaved Buck–Boost DC–DC Power Converter with Continuous Input Current for Fuel Cell Energy Sources: Theoretical Design and Experimental Validation

Mohamed Koundi [1,†], Zakariae El Idrissi [1,*,†], Hassan El Fadil [1], Fatima Zahra Belhaj [1], Abdellah Lassioui [1], Khawla Gaouzi [1], Aziz Rachid [2] and Fouad Giri [3]

[1] ISA Laboratory, ENSA, Ibn Tofail University, Kenitra 14000, Morocco; mohamed.koundi.mk@gmail.com (M.K.); elfadilhassan@yahoo.fr (H.E.F.); fz.blhj@gmail.com (F.Z.B.); abdellah.lassioui@uit.ac.ma (A.L.); khawla.gaouzi@gmail.com (K.G.)
[2] LSIB Laboratory, FST, Hassan II University, Mohammedia 28806, Morocco; rachidaziz03@gmail.com
[3] LAC, UNICAEN, 14000 Caen, France; fouad.giri@unicaen.fr
* Correspondence: zakariae.elidrissi@gmail.com
† These author contribute equally in the paper.

check for updates

Citation: Koundi, M.; El Idrissi, Z.; El Fadil, H.; Belhaj, F.Z.; Lassioui, A.; Gaouzi, K.; Rachid, A.; Giri, F. State-Feedback Control of Interleaved Buck–Boost DC–DC Power Converter with Continuous Input Current for Fuel Cell Energy Sources: Theoretical Design and Experimental Validation. *World Electr. Veh. J.* **2022**, *13*, 124. https://doi.org/10.3390/wevj13070124

Academic Editor: Hang Gao

Received: 9 May 2022
Accepted: 16 June 2022
Published: 7 July 2022

Publisher's Note: MDPI stays neutral with regard to jurisdictional claims in published maps and institutional affiliations.

Abstract: It is well known that the classical topologies of Buck–Boost converters drain pulsating current from the power source. These pulsating currents entail acceleration of the aging rate of the fuel cell. In this paper, we are considering a Buck–Boost DC–DC converter topology featuring continuous input current. The converter interleaved structure ensures the substantial increase in power density compensating power losses related to the converter switching nature. The control objective is to enforce the DC-bus voltage to track its desired value despite load uncertainties and to ensure adequate current sharing between the different parallel modules of the fuel cell interleaved Buck–Boost converter (FC-IBBC). The point is that the internal voltage of the fuel cell is not accessible for measurement. Therefore, the state-feedback control, which consists of nonlinear control laws, is designed on the basis of a nonlinear model of the FC-IBBC system. We formally prove that the proposed controller meets its objectives, i.e., DC-bus voltage regulation and equal current sharing. The theoretical proof relies on the asymptotic stability analysis of the closed-loop system using Lyapunov stability tools. The theoretical results are well confirmed both by simulation, using MATLAB®/Simulink®, and by experimental tests using DS 1202 MicroLabBox.

Keywords: adaptive nonlinear control; DC–DC interleaved Buck–Boost converter; experimental validation; fuel cell

1. Introduction

In the past two decades, clean energy demand has become a worldwide strategic challenge. To meet this challenge, huge financial investments are being made in the technological development of renewable energies, especially fuel cell, solar energy, wind energy, marine energy, and others [1–3]. All sources contribute to reducing CO_2 emissions and reducing global warming effects [4]. In this study, fuel cell energy sources are focused on. A fuel cell is an electrochemical generator, whose electrodes are continuously supplied with fuel and oxidant. In electric vehicles, proton exchange membrane fuel cell (PEMFC) technology is used [5]. Accordingly, proton exchange membranes supply hydrogen, while oxygen is obtained from the air. In most applications, the electrical energy produced by fuel cells is not well shaped for immediate use (e.g., the provided voltage is not constant). To be usable with several loads of different nature, a fuel cell needs to be associated with one or more power converters with appropriate topologies. The converters are required to shape the provided electric energy (see Figure 1).

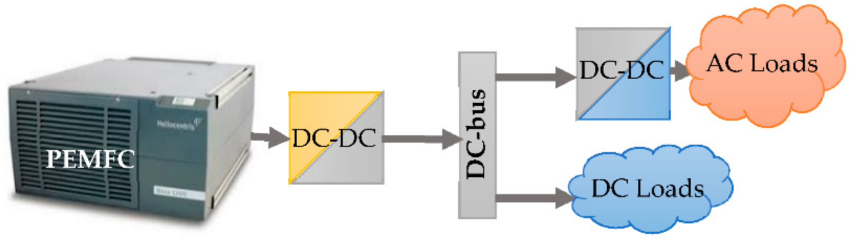

Figure 1. DC-bus voltage for a PEMFC.

Indeed, the static (current-voltage) characteristic of PEMFC, shown in Figure 2, is nonlinear [6,7] and depends on the thermodynamically predicted fuel cell voltage output and the following three majors losses: activation losses (due to electrochemical reaction), ohmic losses (due to ionic electronic condition), and concentration losses (due to mass transport). Therefore, PEMFC systems need to use the DC–DC power converters to supply regulated and stable power to the different loads and equipment [8–21]. Classical DC–DC power converters of Boost and Buck converters are widely used in the fuel cell system [22–25]. The electrical loads in fuel cell systems are generally changing; this is particularly the case in electric vehicle applications.

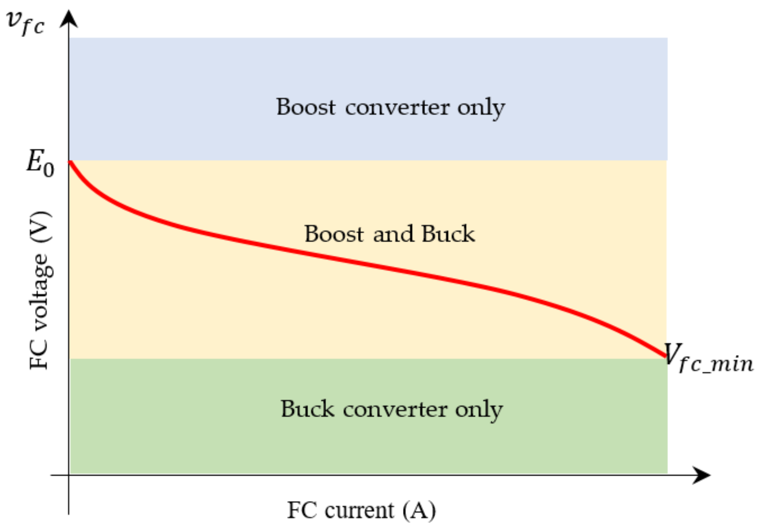

Figure 2. Nonlinear *i-v* characteristic of the fuel cell and use region of DC–DC power converters.

A changing load leads to voltage drops (when the load increases) that need to be compensated for by implementing a step-up converter in the fuel cell systems.

However, this open-loop solution proves only to be satisfactory with small voltage drops. In the presence of wide range variations in the fuel cell voltage, the lowest voltage may become smaller than a third of the nominal open-circuit voltage E_0 [6,26–28]. Then, the solution is to use a Buck converter in the fuel cell system to cope with voltage regulation. It turns out that a fuel cell system must include both Boost and Buck power converters (see Figure 2). Each converter is operated in turn, according to a well defined control strategy that aims at achieving a satisfactory DC-bus voltage regulation.

According to the previous observations, the DC–DC Buck–Boost power converter would be the best interfacing topology for fuel cells as it combines both the Buck mode and Boost mode. Furthermore, the proposed topology of the Buck–Boost converter requires few components, and hence features good reliability [14]. The point is that classical Buck–Boost converter topologies drain pulsating currents from the input power source [29]. Such currents are likely to accelerate the aging rate of the fuel cell [30,31]. To obtain round pulsating currents, power converters can be augmented with input inductors to smooth currents. In this respect, Sepic and Cuk converters are potential solutions to compensate for the pulsating currents in fuel cells. However, these converters require a large number of components, which increases their cost and reduces their reliability [32]. In this paper, we propose a fuel cell system with a Buck–Boost DC–DC converter that features a continuous input current [33,34]. The proposed topology of interleaved Buck–Boost DC–DC power converter features a structure that ensures much higher power density in the switching converters. The interleaving principle consists of connecting a number of converters connected in parallel with an appropriate switching function between transistors. It is shown in many places (e.g., in [35]); DC–DC power converters based on the interleaving technique offer substantial features. Indeed, when the interleaving N module switches phase shift $\frac{2\pi}{N}$, the frequency of the total current ripple is much smaller than that of the current in the various individual modules; specifically, the ratio between both frequencies is less than $\frac{1}{N}$. Therefore, for a given net ripple amplitude and electromagnetic interference specification, the parameter values of the input filter can be made smaller by a factor of $\frac{1}{N}$. On the other hand, for a fixed net frequency f, the switching frequency in the individual modules is reduced to $\frac{f}{N}$, leading to a substantial reduction in the switching losses. Furthermore, splitting the total power on the N paralleled converters entails the division N of the input/output current in each individual module. Accordingly, the current ripple can be reduced N times, and so can the inductance value in each module, consequently, allowing a smaller size converter under current passive component technology. Ensuring a satisfactory energy exchange between the FC-IBBC and the load necessitates the design and implementation of a controller with the following satisfactory performances: stability, reliability, robustness, etc. In this respect, several controllers have been proposed in the literature for the association of the FC and the power converter.

In [9], a (linear/nonlinear/adaptive . . .) controller was proposed for a multi-device multi-phase interleaved Buck–Boost converter, which meets the constraint of current continuity of the fuel cell. The point with the considered architecture is the high number of the converter components, which entails the high cost and large size of the converter, and greater energy losses.

In [10], a classical interleaved Buck–Boost converter (with $N = 6$) has been highlighted and a (linear/nonlinear/adaptive . . .) controller has been proposed. A drawback of the proposed solution is that actuation is performed by transistors with a gap between them, in order to ensure the continuity of the current of the fuel cell.

The authors [15–17] present multi-level architectures of Boost-type power converters; these converters are not suitable with the fuel cell as a power source, when one wants a converter output voltage lower than V_{fc_min} (minimum fuel cell voltage). However, they can be used in other applications.

In [33], DC-bus voltage in a mono-module ($N = 1$) FC-IBBC system was indirectly dealt with by regulating the inductor current at a given reference. The indirect control strategy was motivated by the non-minimum phase nature of the involved Buck–Boost converter. The study emphasized the importance of conveniently sizing the converter components (especially capacitance and inductance) to avoid excessive peaks in current ripples.

The present work is focused on the problem of controlling multiple-module ($N > 1$) FC-IBBC systems. We seek the achievement of the following control objectives: (i) tight regulation of the DC-bus voltage, (ii) equal current sharing between different parallel modules of the IBBC, and (iii) asymptotic stability of the closed-loop system. In addition to the (multiple-module) interleaved structure of the converter, the system complexity also lies in the nonlinear non-minimum phase dynamics, and the load variation and uncertainty. The control problem at hand is coped with by developing a nonlinear controller that is designed using the backstepping technique, on the basis of the nonlinear system model. The adaptive feature reflects the controller's ability to perform an online estimate of load resistance (a part of the system), despite parameter uncertainty. To this end, estimating the load resistance entails the reduction in sensors and, consequently, the increase in control system reliability and the reduction in its size. The effectiveness of the proposed controller is first established by a theoretical analysis of the closed-loop control stability.

The outcome of the theoretical analysis is then confirmed both by the simulation results and by experimental tests.

The rest of the paper is organized as follows: the system of interest, including a PEMFC and an interleaved DC–DC Buck–Boost power converter is described, modelled, and analyzed in Section 2; in Section 3, we present an adaptive state-feedback controller; the simulation and experimental results are presented in Section 4. A conclusion and reference list conclude the paper.

2. Modelling and Analysis of Fuel-Cell in Association with Buck–Boost Converter

2.1. System Presentation

The FC-IBBC system of interest is depicted in Figure 3. It is constituted of a fuel cell (FC), an interleaved Buck–Boost converter (IBBC), and a load. The FC is represented by its equivalent electric circuit [36,37]. The IBBC contains N modules connected in parallel, operating according to the pulse width modulation (PWM) principal. The parallel modules share a common DC-bus with the load, which is a resistance R. The FC is characterized by an open-circuit voltage E_0, an ohmic resistance R_o, an equivalent electrical capacitance C_{fc}, and a series equivalent resistance of activation and concentration resistance R_{ac}. Each Buck–Boost module consists of an inductor L_k with its equivalent series resistance r_k, a filtering capacitor C in parallel with the switches and diodes, a static switch S_k controlled by the binary input signal u_k, and a diode D_k ($k = 1, \ldots, N$). Each diode anode is connected to the same point with the load represented by a pure resistance R, according to the input impedance of the DC-bus. This impedance is actually unknown because it depends on the power demand. This uncertainty, together with other parameter uncertainties, will be investigated in the next section.

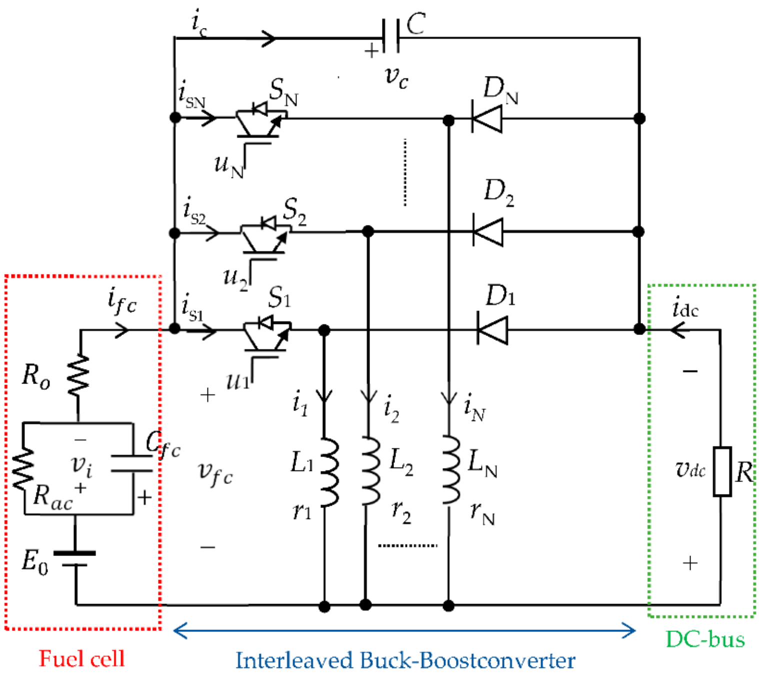

Figure 3. Fuel cell association with an interleaved Buck–Boost DC–DC converter (IBBC).

2.2. System Modelling

Applying Kirchhoff's laws to the systems of Figure 3, we obtain the following bilinear model:

$$\frac{di_k}{dt} = -\frac{r_k}{L_k} i_k - \frac{1}{L_k}(1-u_k)v_c + \frac{1}{L_k} v_{fc} \tag{1}$$

$$\frac{dv_c}{dt} = \frac{1}{C}\Sigma_{k=1}^{N}(1-u_k)i_k + \frac{1}{RC}(v_{fc} - v_c) \tag{2}$$

$$\frac{dv_i}{dt} = -\frac{1}{\tau_{fc}}v_i + \frac{1}{C_{fc}}i_{fc} \tag{3}$$

$$i_{fc} = \frac{R}{R+R_o}\sum_{k=1}^{N} i_k + \frac{1}{R+R_o}(E_0 - v_c - v_i) \tag{4}$$

$$v_{fc} = E_0 - R_o i_{fc} - v_i \tag{5}$$

$$v_{dc} = v_c - v_{fc} \tag{6}$$

with $k = 1, \ldots, N$, where u_k denotes the binary control signal, taking values 1 or 0, N is the number of the parallelly connected Buck–Boost modules composing the IBBC; $\tau_{fc} = C_{fc}R_{ac}$ is the fuel cell electrical time constant. This model is useful for circuit simulation purposes but is not suitable for the controller design because it involves binary control inputs u_k. For the control design purpose, the following averaged model is obtained using the averaging technique [38], which will prove to be useful:

$$\frac{dx_{1k}}{dt} = -\frac{r}{L}x_{1k} - \frac{1}{L}(1-\mu_k)x_2 + \frac{1}{L}\overline{v}_{fc} \tag{7}$$

$$\frac{dx_2}{dt} = \frac{1}{C}\sum_{k=1}^{N}(1-\mu_k)x_{1k} + \frac{1}{RC}(\overline{v}_{fc} - x_2) \tag{8}$$

$$\frac{dx_3}{dt} = -\frac{1}{\tau_{fc}}x_3 + \frac{1}{C_{fc}}\bar{i}_{fc} \tag{9}$$

$$\bar{i}_{fc} = \frac{R}{R+R_o}\sum_{k=1}^{N} x_{1k} + \frac{1}{R+R_o}(E_0 - x_2 - x_3) \tag{10}$$

$$\overline{v}_{fc} = E_0 - R_o\bar{i}_{fc} - x_3 \tag{11}$$

$$\overline{v}_{dc} = x_2 - \overline{v}_{fc} \tag{12}$$

where the state variables $x_{1k};\ (k = 1, \ldots, N)$ designate the average values over the switching period of the inductor current of each module (i_k), x_2 and x_3 designate the average values of the capacitor voltage (v_c) and the FC internal voltage (v_i), respectively. The quantity $\mu_k \in [0, 1]$, which denotes the duty ratio function of the PWM control signal u_k, acts as the control input for each IBBC module. The quantities $\overline{v}_{fc}$, $\bar{i}_{fc}$ and $\overline{v}_{dc}$ respectively denote the average values of the fuel cell voltage v_{fc}, the fuel cell current i_{fc}, the DC-bus voltage v_{dc}. For simplicity, we assumed the IBBC modules to be identical, leading to equal inductances and their ESR in (7), i.e., $L_k = L$ and $r_k = r$, $k = 1, \ldots, N$.

2.3. System Steady State Analysis

V_d denotes the desired output voltage in the steady state. The (average) DC components are obtained by setting to zero all the state variable derivatives in (7–9). Doing so, we obtain the following equations from (9):

$$V_d = \frac{UE_0}{1-U} \times \eta \tag{13}$$

$$I_d = \frac{V_d}{NR(1-U)} \tag{14}$$

$$I_{fc} = \frac{V_d}{R}\frac{U}{(1-U)} \tag{15}$$

$$V_{fc} = E_0 - (R_o + R_{ac})I_{fc} \tag{16}$$

$$V_c = V_d + V_{fc} \tag{17}$$

$$\text{with } \eta = \frac{R(1-U)^2}{R(1-U)^2 + (R_o + R_{ac})U^2 + \frac{r}{N}} \tag{18}$$

where V_c, V_{fc}, I_d, I_{fc} and U denote the steady-state values of the various variables, i.e., capacitor voltage, fuel cell voltage, inductor current in each IBBC branch, fuel cell current, the duty ratio of each IBBC module.

From (13), the conversion ratio of the FC-IBBC system is given by

$$G_v(U) = \frac{V_d}{E_0} = \frac{U}{1-U} \times \eta \tag{19}$$

Remark 1. *Equation (18) shows that the interleaving nature improves the conversion ratio as the ideality factor η in (19) increases with N. On the other hand, (18) also shows that η depends on fuel cell parameters (R_o, R_{ac}) and the inductance ESR. For r, the smaller it is (r, R_o, R_{ac}), the larger the conversion ratio.*

Remark 2. *In ideal conditions, i.e., $R_o = R_{ac} = r = 0$, one has $\eta = 1$, which gives $G_{vi} = \frac{U}{1-U}$. The latter represents the classical conversion ratio for the traditional Buck–Boost converter. When the duty ratio U varies between 0 and 1, the output voltage could be smaller or larger than the input voltage E_0; this justifies the Buck–Boost designation of the converter. It is worth noting that the main feature of the proposed Buck–Boost is the continuous current provided by the fuel cell.* Figure 4 *illustrates the conversion ratio versus duty ratio in the presence of the variations in the load resistance R and parasitic parameters (R_o, R_{ac}, r).*

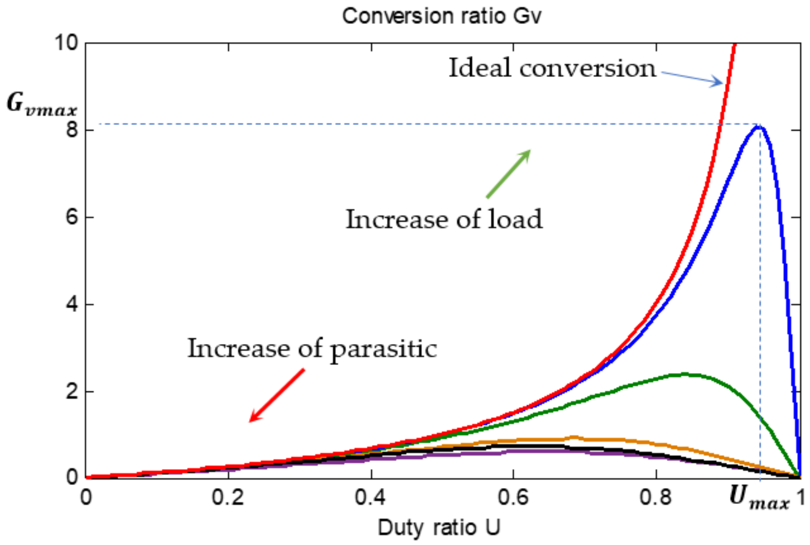

Figure 4. Conversion ratio versus resistance load and parasitic parameters.

The maximum conversion ratio G_{vmax} and its corresponding duty ratio U_{max} are obtained from (18), (19), which is as follows:

$$U_{max} = \frac{-(r + NR_o - \sqrt{(r+NR)(r+N(R_{ac}+R_o))})}{N(R_{ac}+R_o-R)} \tag{20}$$

$$G_{vmax} = \frac{RU_{max}(1-U_{max})}{R(1-U_{max})^2 + (R_o+R_{ac})U_{max}^2 + \frac{r}{N}} \tag{21}$$

3. Nonlinear State Feedback Controller

In this section, we aim at designing an appropriate controller for the nonlinear system (1–3), on the basis of the nonlinear model (7–9). The model complexity lies in its nonlinearity and the uncertainty of the load resistance. The control objectives are the following:

(i) Tight regulation of output DC-bus voltage despite load uncertainty.

(ii) Equal current sharing between IBBC branches, i.e., the inductor currents should be equal to each other in order to avoid overloading one of the modules, especially when supplying heavy loads. This property entails the reduction in the current ripple, which is beneficial for fuel cells.

(iii) Asymptotic stability of the closed-loop system.

Note that load resistance R uncertainty results from the fact that the load usually varies in practical applications. This model uncertainty will now be solved by providing the controller with adaptive capability. To this end, the controller to be designed will be equipped with a parameter estimator providing online estimates of the unknown parameter $\theta = \frac{1}{R}$.

The first control objective amounts to enforcing the DC-bus voltage v_{dc} to track its desired value V_d. The point is that the Buck–Boost converter is of a non-minimum phase nature [39] and so perfect tracking of the arbitrary reference signals is not achievable. To avoid this issue, we seek the achievement of the above objective indirectly. Specifically, we consider the inductor currents x_{1k}, in IBBC modules, as output signals and aim at enforcing them to track reference signals, denoted I_d. The latter is chosen so that if $x_{1k} = I_d$ then $v_{dc} = V_d$. From (13), (14), we obtain the following relationship between the desired current value I_d and the desired voltage V_d:

$$I_d = \frac{V_d}{N}\left(\eta_0 \frac{V_d}{E_0} + 1\right)\frac{1}{R} = K\theta \tag{22}$$

with

$$K = \frac{V_d}{N}\left(\eta_0 \frac{V_d}{E_0} + 1\right) \tag{23}$$

where $\eta_0 \geq 1$ is an ideality factor introduced to take into account all losses, including switching losses in the converters and the losses in the inductances ESR and the losses in the fuel cell resistance (see Section 2.3). Since θ is unknown, one must introduce the estimated value of I_d.

$$\hat{I}_d = K\hat{\theta} \tag{24}$$

where $\hat{\theta}$ is an online estimate of $\theta = \frac{1}{R}$ provided by a parameter estimator yet to be determined. The following state tracking errors are introduced:

$$e_{1k} = x_{1k} - \hat{I}_d; \quad k = 1, \ldots, N \tag{25}$$

Clearly, the objective of regulating the DC-bus voltage v_{dc} to its reference value V_d amounts to regulating the errors e_k to zero. To meet the last requirement, we will apply the backstepping design technique. Accordingly, we first highlight the dynamics of e_k by differentiation (25), with respect to time, and using (7) as follows:

$$\dot{e}_{1k} = -\frac{r}{L}x_{1k} - \frac{1}{L}(1-\mu_k)x_2 + \frac{1}{L}\overline{v}_{fc} - K\dot{\hat{\theta}} \tag{26}$$

To make the errors e_{1k} asymptotically vanish, one can enforce their dynamics to behave as follows:

$$\dot{e}_{1k} = -c_{1k}e_{1k} + e_2 \tag{27}$$

where $c_{1k} > 0$ are design parameters, and

$$e_2 = x_2 - x_{2d} \tag{28}$$

is the error between the capacitor voltage x_2 and x_{2d}, which is its desired value to be defined later.

Combining (26) with (27), one can obtain the following control laws for the FC-IBBC system:

$$\mu_k = 1 + \frac{L}{x_2}\left(-c_{1k}e_{1k} + e_2 + \frac{r}{L}x_{1k} - \frac{1}{L}\overline{v}_{fc} + K\dot{\hat{\theta}}\right) \quad (29)$$

Using (8) and (28), it is readily checked that the dynamics of e_2 are governed by the following equation:

$$\dot{e}_2 = \frac{1}{C}\sum_{k=1}^{N}(1-\mu_k)x_{1k} + \frac{1}{C}(\overline{v}_{fc} - x_2)(\widetilde{\theta} + \hat{\theta}) - \dot{x}_{2d} \quad (30)$$

The third control objective ensures asymptotic stability of the error system with state variables (e_{1k}, e_2). This requirement will be enforced by conveniently selecting the still free quantities x_{2d} and $\hat{\theta}$, in (26) and (29). To this end, we consider the following Lyapunov function candidate [40] for the $(e_{1k}, e_2, \widetilde{\theta})$ system as follows:

$$V_1 = \frac{1}{2}\left(\sum_{k=1}^{N} e_{1k}^2 + e_2^2 + \frac{1}{\gamma}\widetilde{\theta}^2\right) \quad (31)$$

with $\widetilde{\theta} = \theta - \hat{\theta}$ being the estimation error and $\gamma > 0$ any real scalar, which is called parameter adaptation gain, to be chosen by the designer. The time-derivative of V_1 gives the following equation, using (27):

$$\dot{V}_1 = -\sum_{k=1}^{N} c_{1k}e_{1k}^2 + e_2(\sum_{k=1}^{N} e_{1k} + \dot{e}_2) + \frac{1}{\gamma}\widetilde{\theta}\dot{\widetilde{\theta}} \quad (32)$$

Using (32), it follows from (32).

$$\dot{V}_1 = -\sum_{k=1}^{N} c_{1k}e_{1k}^2 + e_2(\sum_{k=1}^{N} e_{1k} + \frac{1}{C}\sum_{k=1}^{N}(1-\mu_k)x_{1k} + \frac{\hat{\theta}}{C}(\overline{v}_{fc} - x_2) - \dot{x}_{2d}) + (-\frac{\dot{\hat{\theta}}}{\gamma} + \frac{1}{C}(\overline{v}_{fc} - x_2)e_2)\widetilde{\theta} \quad (33)$$

Equation (33) shows that $\dot{V}_1$ can be made negative definite, letting $\dot{x}_{2d}$ and $\dot{\hat{\theta}}$ be the following:

$$\begin{cases} \sum_{k=1}^{N} e_{1k} + \frac{1}{C}\sum_{k=1}^{N}(1-\mu_k)x_{1k} + \frac{\hat{\theta}}{C}\left(\overline{v}_{fc} - x_2\right) \\ \qquad -\dot{x}_{2d} = -c_2 e_2 \\ -\frac{\dot{\hat{\theta}}}{\gamma} + \frac{1}{C}\left(\overline{v}_{fc} - x_2\right)e_2 = 0 \end{cases} \quad (34)$$

where $c_2 > 0$ is a design parameter. From the second part of (34), we obtain the following parameter adaptive control law:

$$\dot{\hat{\theta}} = -\dot{\widetilde{\theta}} = \frac{\gamma}{C}(\overline{v}_{fc} - x_2)e_2 \quad (35)$$

using the fact that $\dot{\widetilde{\theta}} = -\dot{\hat{\theta}}$, assuming that the uncertain parameter θ is time-invariant or subject to infrequent step changes. In addition, using (28), the first part of (34) implies the following desired value x_{2d}:

$$x_{2d} = \frac{1}{s + c_2}[\sum_{k=1}^{N} c_{1k}e_{1k} + c_2 x_2 + \frac{1}{C}\sum_{k=1}^{N}(1-\mu_k)x_{1k} + \frac{\hat{\theta}}{C}(\overline{v}_{fc} - x_2)] \quad (36)$$

with s being the Laplace variable.

Finally, using (36) and (35), the control law (29) becomes the following equation:

$$\mu_k = 1 + \frac{L}{x_2}\left(-c_{1k}e_{1k} + e_2 + \frac{r}{L}x_{1k} - \frac{1}{L}\overline{v}_{fc} + \frac{K\gamma}{C}(\overline{v}_{fc} - x_2)e_2\right) \quad (37)$$

The main result of this subsection is now summarized in the following Theorem 1.

Theorem 1. *Consider the closed-loop system consisting of a fuel cell interleaved Buck–Boost converter system described by (7)–(9), subject to load resistor uncertainty, and the controller consisting of the adaptive control law (37), the parameter update law (35), and the desired trajectory* x_{2d} *of the capacitor voltage (36). Then, one has the following:*

(1) The closed-loop system with state variables (e_{1k}, e_2) *is globally asymptotically stable around the origin;*
(2) The tracking errors e_{1k} *converge asymptotically to zero, implying proper current sharing between the modules;*
(3) The estimation error $\widetilde{\theta} = \theta - \hat{\theta}$ *converges to zero and, consequently, the estimated reference current* $\hat{I}_d$ *converges to its real value,* I_d*. It turns out that the tracking error* $\varepsilon = v_{dc} - V_d$ *converges to zero, ensuring tight regulation of the DC-bus voltage.*

Proof. First, a state-space representation of the closed-loop system should be obtained, substituting $\dot{x}_{2d}$ obtained from (34) in (32) yields.

$$\dot{e}_2 = -c_2 e_2 - \sum_{k=1}^{N} e_{1k} + \frac{1}{C}(\overline{v}_{fc} - x_2)\widetilde{\theta} \tag{38}$$

This together with (27) and (35) describes the closed-loop system, which is rewritten as follows:

$$\dot{e}_{1k} = -\sum_{k=1}^{N} e_{1k} c_{1k} + e_2; k = 1, \ldots, N \tag{39}$$

$$\dot{e}_2 = -c_2 e_2 - \sum_{k=1}^{N} e_{1k} + \frac{1}{C}(\overline{v}_{fc} - x_2)\widetilde{\theta} \tag{40}$$

$$\dot{\widetilde{\theta}} = -\dot{\hat{\theta}} = -\frac{\gamma}{C}(\overline{v}_{fc} - x_2)e_2 \tag{41}$$

Part 1: Now, substituting the right side of (34) in (33), one obtains the following derivative of the Lyapunov function:

$$\dot{V}_1 = -\sum_{k=1}^{N} c_{1k} e_{1k}^2 - c_2 e_2^2 \tag{42}$$

In view of (30), (38) shows that $\dot{V}_1$ is a negative semi-definite function of the state vector $(e_{1k}, e_2, \widetilde{\theta})$. Therefore, $(e_{1k}, e_2, \widetilde{\theta}) = (0,\ 0,\ 0)$ is globally stable.

Part 2: After applying LaSalle's invariance theorem [41], it further follows that the state vector $(e_{1k}, e_2, \widetilde{\theta})$ converges to the largest invariant set of (40–42) contained in the set $\left\{(e_{1k}, e_2, \widetilde{\theta}) \in IR^{N+2} / \dot{V}_1 = 0\right\}$. Given (38), the invariant set denoted M is contained in $M_0 \overset{\text{def}}{=} \left\{(e_{1k}, e_2, \widetilde{\theta}) \in IR^{N+2} / (e_{1k}, e_2) = 0\right\}$, which shows that

$$\lim_{t\to\infty}(e_{1k}(t), e_2(t)) = 0 \tag{43}$$

which in turn, using (40) and the fact that $\lim_{t\to\infty}(\dot{e}_{1k}(t), \dot{e}_2(t)) = 0$, shows that

$$\lim_{t\to\infty}\widetilde{\theta}(t) = 0 \tag{44}$$

This implies that $\hat{\theta}$ converges to its true value θ and, in turn, gives $\hat{I}_d \to I_d$, which also implies, using (25), that

$$\lim_{t\to\infty} x_{1k}(t) = 0 = I_d \tag{45}$$

From Figure 3, in the steady-state, the averaged current in each transistor is

$$I_{Sk} = \lim_{t\to\infty} \mu_k x_{1k} = U I_d\ ; \quad k = 1, \ldots, N \tag{46}$$

which, using (14) and (15), gives

$$I_{Sk} = \frac{I_{fc}}{N}; k = 1, \ldots, N \tag{47}$$

This clearly shows that the fuel cell current is equally shared between the IBBC branches. This implies that the objective of proper current sharing between the modules is ensured.

Part 3: We have just shown that $\hat{I}_d$ converges towards its true value I_d. We will now demonstrate that the DC-bus voltage v_{dc} converges to its desired value V_d.

From (8), it follows in the steady-state, using (12), that

$$\lim_{t \to \infty} \overline{v}_{dc}(t) = R(1 - U)NI_d \tag{48}$$

which implies, using (14), that

$$\lim_{t \to \infty} \overline{v}_{dc}(t) = V_d \tag{49}$$

This shows that the objective of tight regulation of the DC-bus voltage is also achieved; the proof of Theorem 1 is then completed. □

Remark 3. *The nonlinear controller composed of the adaptive control law (37) and the parameter update law (35) looks similar to a classic cascade control architecture consisting of an inner current loop and an outer voltage loop. In this case, the control law (37) is considered as an inner loop for each IBBC branch, while (22), (23) and (35) are considered as an outer loop for all branches. Figure 5 illustrates a simplified architecture of the proposed control approach.*

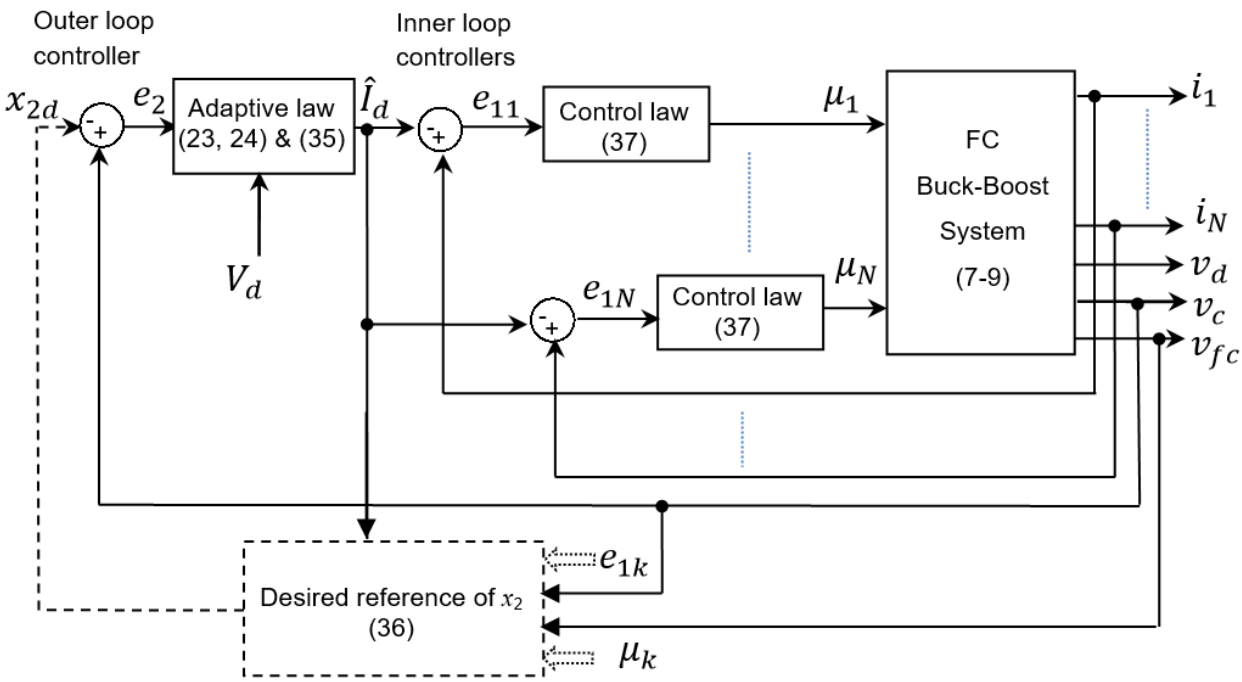

Figure 5. Nonlinear cascade control architecture.

For convenience, the FC-IBBC system is summarized, along with the adaptive controller in Table 1.

Table 1. Nonlinear adaptive controller.

FC-IBBC system	$\frac{dx_{1k}}{dt} = -\frac{r}{L}x_{1k} - \frac{1}{L}(1-\mu_k)x_2 + \frac{1}{L}\overline{v}_{fc}$	(7)
	$\frac{dx_2}{dt} = \frac{1}{C}\sum_{k=1}^{N}(1-\mu_k)x_{1k} + \frac{1}{RC}(\overline{v}_{fc} - x_2)$	(8)
	$\frac{dx_3}{dt} = -\frac{1}{\tau_{fc}}x_3 + \frac{1}{C_{fc}}\overline{i}_{fc}$	(9)
	where $k = 1, \ldots, N$;	
Adaptive control laws	$K = \frac{V_d}{N}\left(\eta_0\frac{V_d}{E_0} + 1\right)$	(23)
	$\hat{I}_d = K\hat{\theta}$	(24)
	$e_{1k} = x_{1k} - \hat{I}_d$	(25)
	$e_2 = x_2 - x_{2d}$	(28)
	$x_{2d} = \frac{1}{s+c_2}\left[\sum_{k=1}^{N}c_{1k}e_{1k} + c_2x_2 + \frac{1}{C}\sum_{k=1}^{N}(1-\mu_k)x_{1k} + \frac{\hat{\theta}}{C}\left(\overline{v}_{fc} - x_2\right)\right]$	(36)
	$\mu_k = 1 + \frac{L}{x_2}\left(-c_{1k}e_{1k} + e_2 + \frac{r}{L}x_{1k} - \frac{1}{L}\overline{v}_{fc} + \frac{K\gamma}{C}(\overline{v}_{fc} - x_2)e_2\right)$	(37)
Adaptive law	$\dot{\hat{\theta}} = \frac{\gamma}{C}(\overline{v}_{fc} - x_2)e_2$	(35)
Design parameters	$\eta_0 \geq 1$; $V_d > 0$; $\gamma > 0$; $c_{1k} > 0$; $c_2 > 0$;	

4. Simulation and Experimental Results

The adaptive nonlinear controller developed in this paper for the FC-IBBC system will now be validated both by simulation and by experiments. Simulation is carried out using the Matlab®/Simulink® SimPower toolbox, and the experiments are performed using a laboratory prototype based on the Dspace DS1202 card.

4.1. Simulation Results

The fuel cell parameters are those of the Ballard Nexa 1200 fuel cell module, which has a rated power of 1.2 kW. Figure 5 describes the simulation bench of the controlled system FC-IBBC. The controlled system characteristics are listed in Table 2. The adaptive control design parameters are listed in Table 3.

Table 2. Controlled system parameters.

	Parameter Designation	Value
Fuel Cell	FC open circuit voltage	$E_0 = 28.3$ V
	FC internal capacitor	$C_{fc} = 130$ F
	Association of the activation and concentration resistances	$R_{ac} = 0.155\ \Omega$
	Ohmic resistance	$R_O = 2.89$ mΩ
IBBC	Number of IBBC	$N = 3$
	Filtering inductance	$L_1 = L_2 = L_3 = 1$ mH
	Filtering capacitor	$C = 68$ µF
	ESR of the inductance	$r_1 = r_2 = r_3 = 0.2\ \Omega$
	Switching frequency	$f_s = 20$ kHz

Table 3. The design control parameters.

Parameter	Value
$C_{11} = C_{12} = C_{13}$	6000
C_2	10,000
γ	0.0025
η_0	1

Figures 6–16 show the resulting control performances of the fuel cell interleaved Buck–Boost converter system.

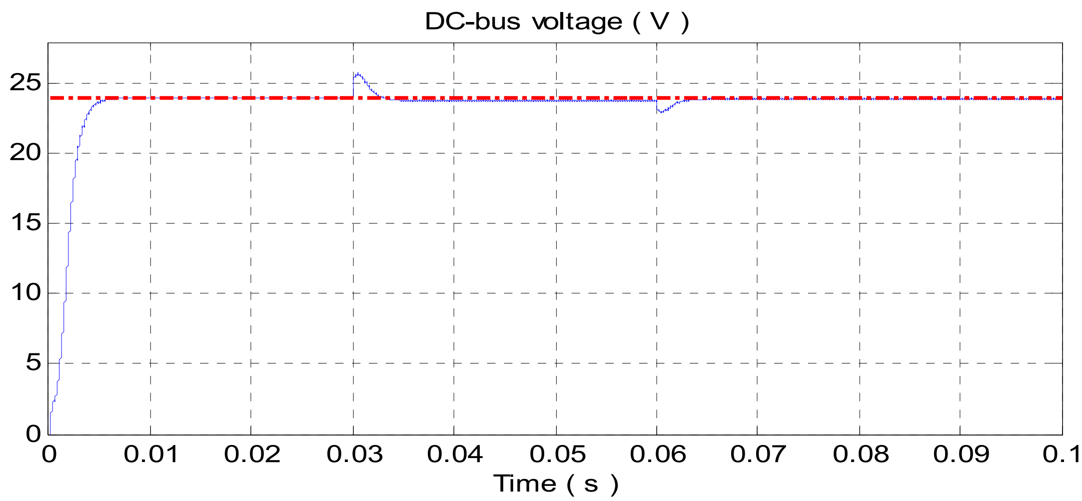

Figure 6. Voltage measurement of v_{dc} and its reference signal V_d.

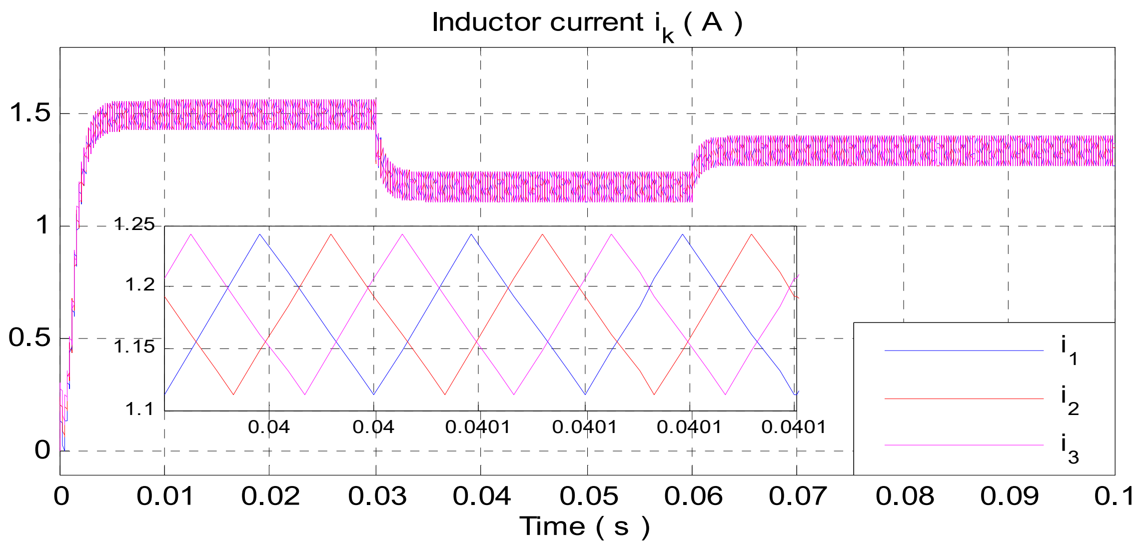

Figure 7. Inductance currents i_k of IBBC.

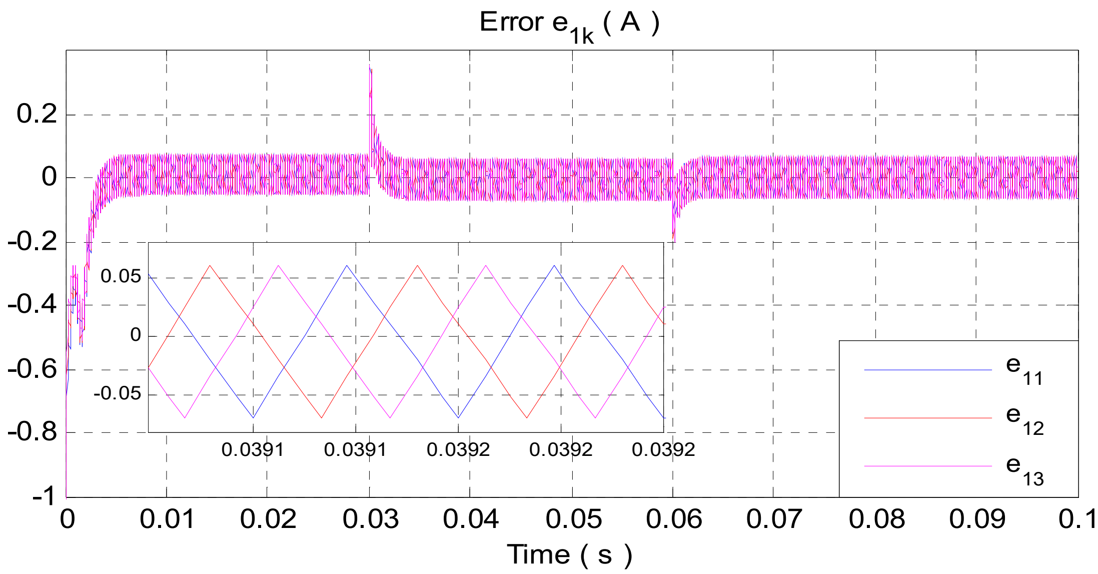

Figure 8. Error e_{1k} between inductance current in each IBBC branch and its reference.

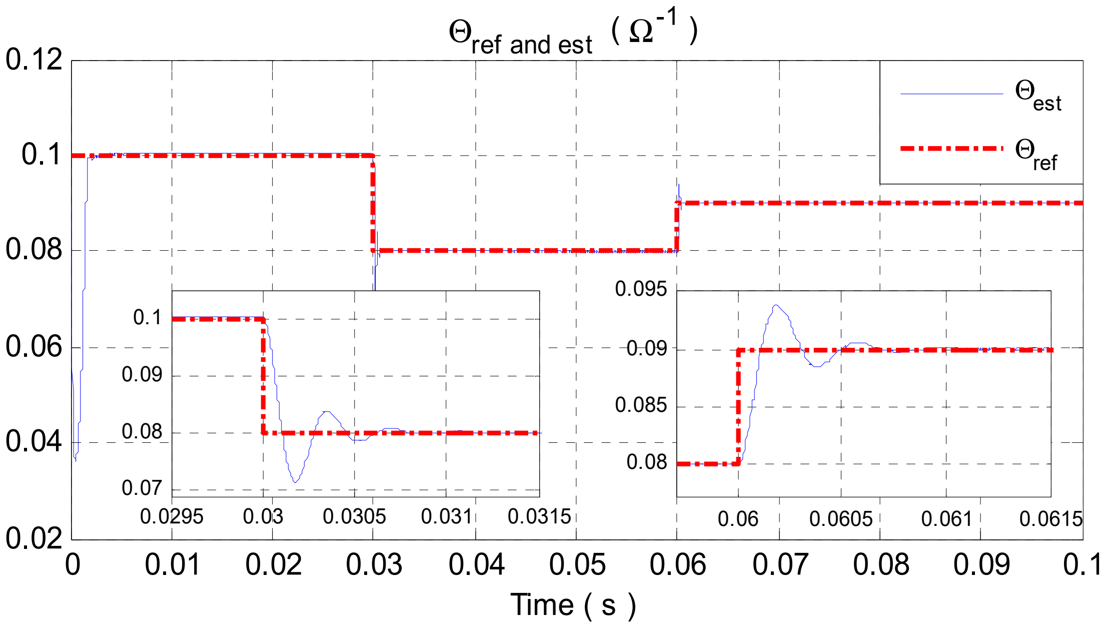

Figure 9. Estimate unknown parameter θ and its reference.

Figure 6 illustrates the voltage measurement of v_{dc} and its reference signal V_d. In this figure, one can observe that the controller behavior is satisfactory. Indeed, the DC-bus v_{dc} perfectly tracks its reference V_d. The overshoot is 0 at t_0 and 5% of V_d at the instant of change in the load, the system response time is less than 5 ms.

Figure 7 shows that the inductance currents are equal to the variation in the load. So, the equal current sharing between the IBBC branches is ensured.

Figure 12 illustrates the capacitor voltage v_c. Figure 8 shows the error e_{1k} between the inductance current in each IBBC branch and its reference. The figure clearly shows that the error e_{1k} converges to zero, despite load variations. The signal ripple is tolerable, as it is less than 0.12A.

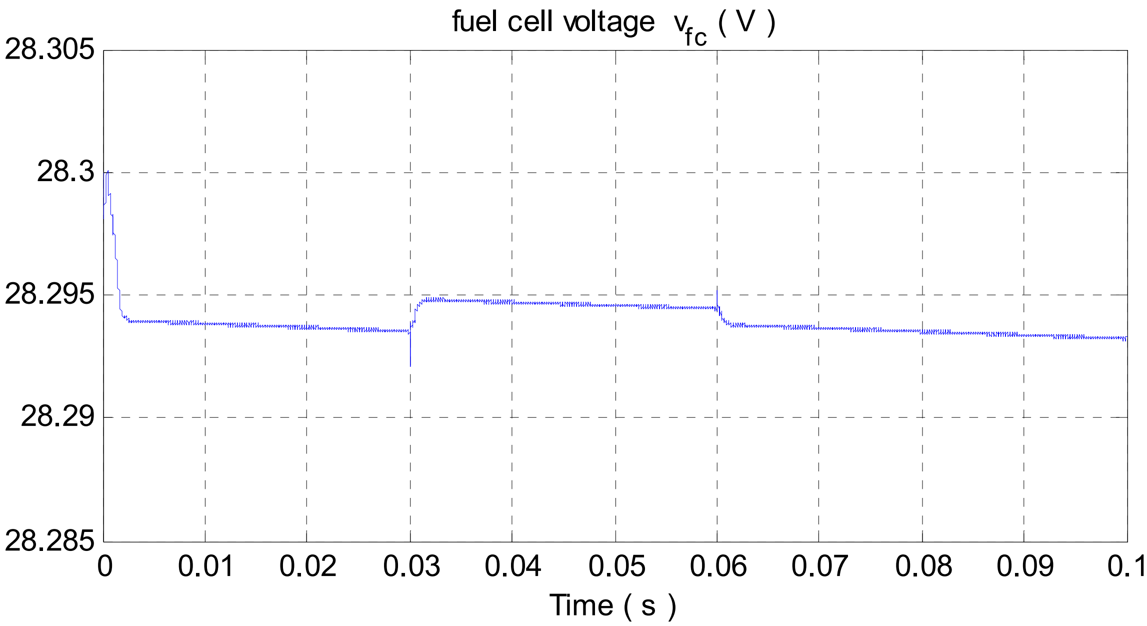

Figure 10. Fuel cell voltage v_{fc}.

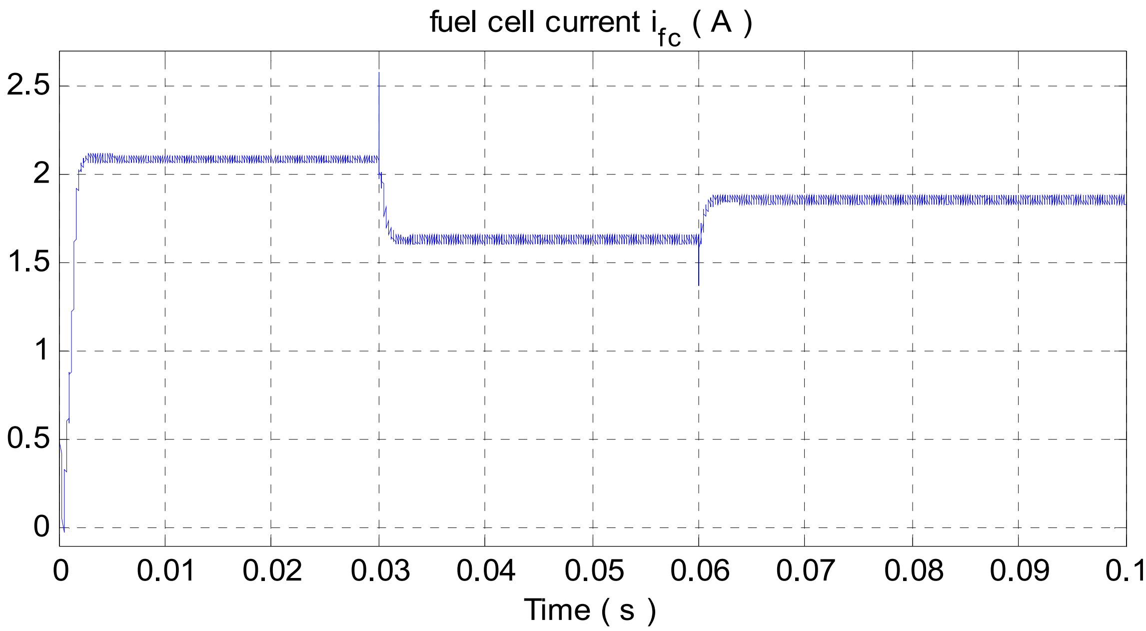

Figure 11. Fuel cell current i_{fc}.

Figure 9 shows that the online estimate of the unknown parameter θ converges to its true value.

Figures 10 and 11 respectively show the behavior of the voltage v_{fc} and current i_{fc} of the fuel cell in the presence of load variations. We can observe that the current of the fuel cell is continuous, which is beneficial for the fuel cell.

Figure 13 shows the error e_2 between the capacitor voltage x_2 and its desired value x_{2d}. Clearly, e_2 is well regulated to zero, despite the variation in the load.

Figure 14 shows the FC internal voltage v_i; one should note that the value of v_i is low because its charge rate is very high. The value of v_i also represents the discharge of hydrogen H_2 in the fuel cell.

Figures 15 and 16 show the control signals μ_{1k} and the PWM signals, with a switching frequency of 20 kHz.

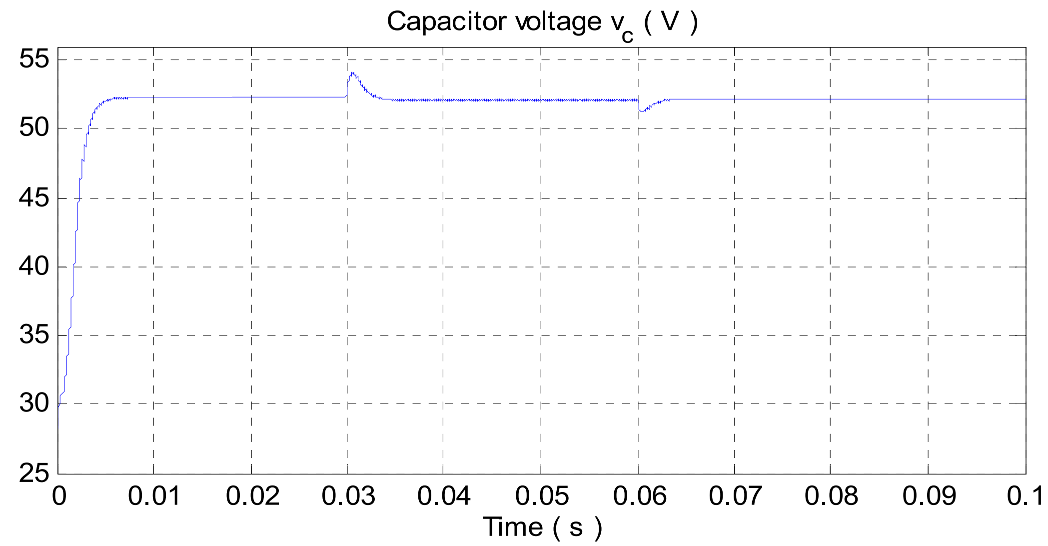

Figure 12. Capacitor voltage v_c.

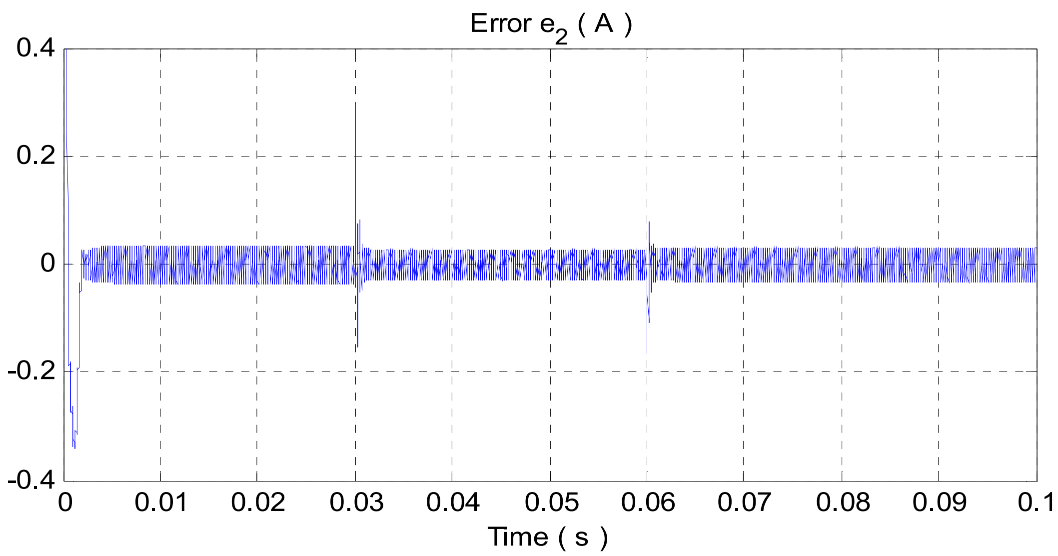

Figure 13. Error e_2 between the capacitor voltage v_c and its desired value x_{2d}.

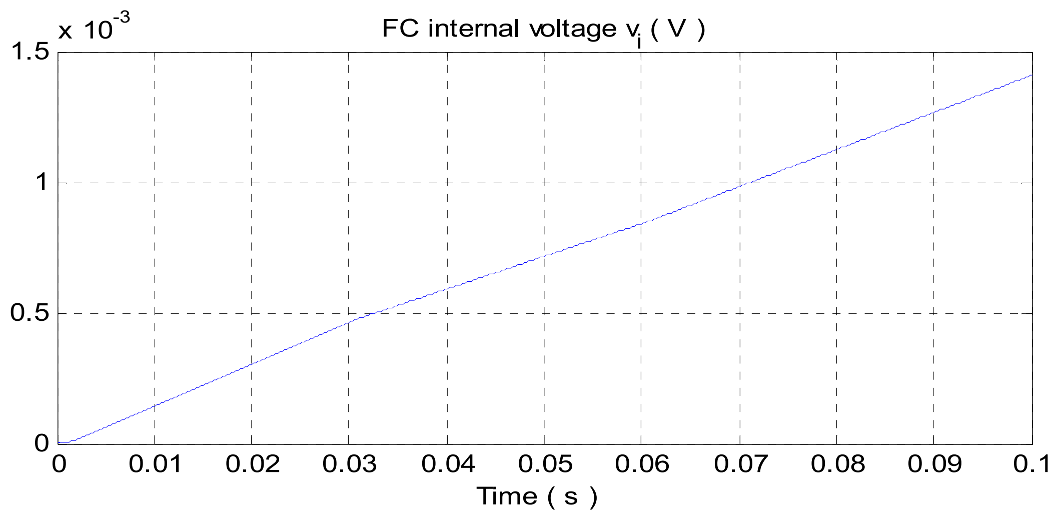

Figure 14. FC internal voltage v_i.

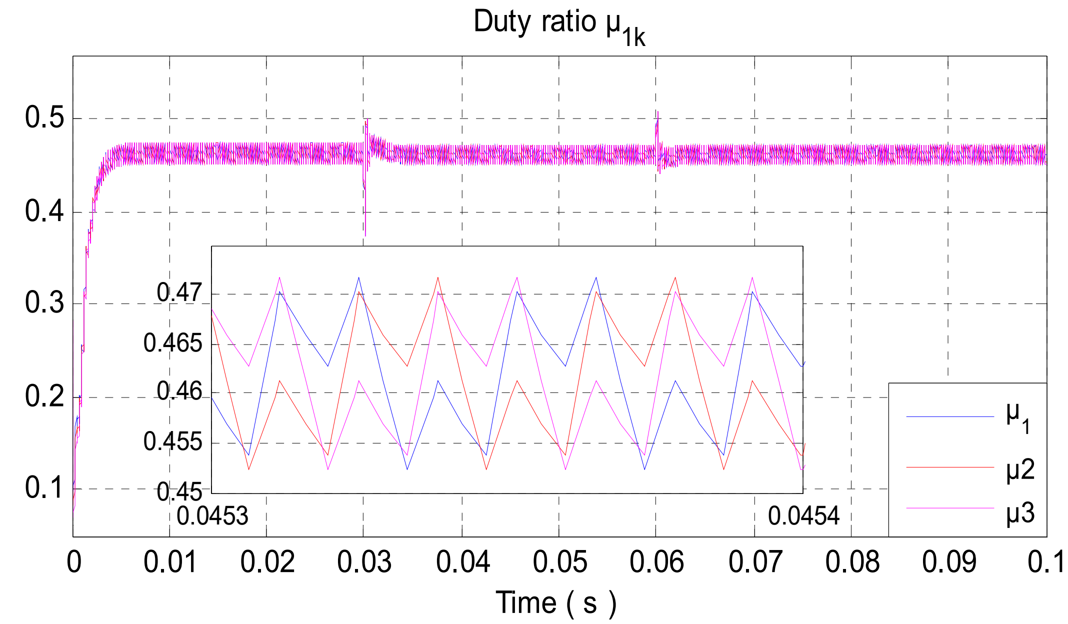

Figure 15. Control signals μ_{1k} with zoom.

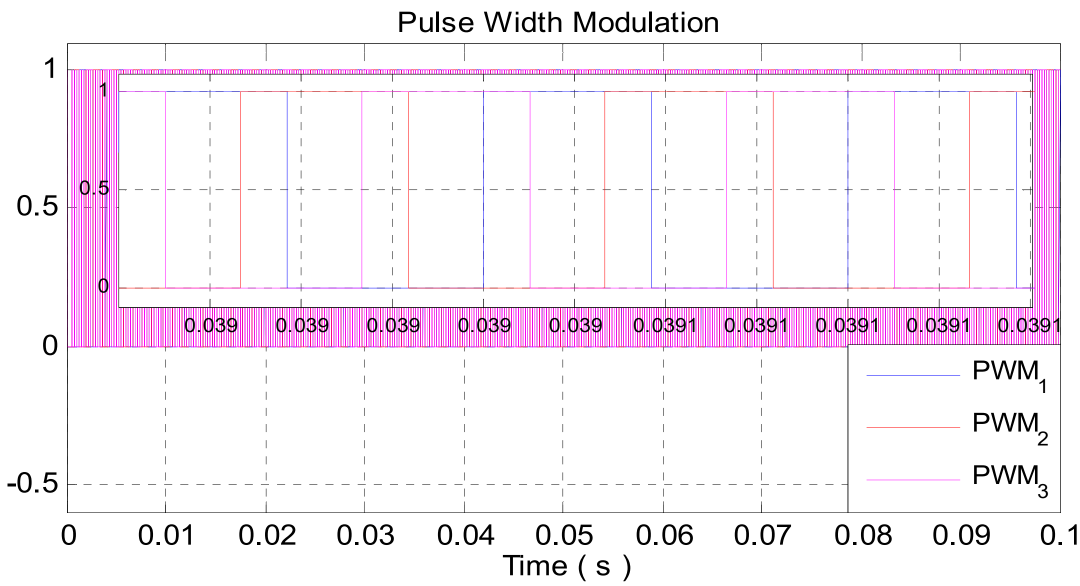

Figure 16. Pulse width modulation of IBBC with zoom.

4.2. Experimental Results

The considered experimental test bench of the fuel cell interleaved Buck–Boost converter system is shown by Figure 17. The adaptive state-feedback controller of Table 2 is implemented using dSPACE 1202 and Control Desk®/software®. The testbed consists essentially of the following elements:

Ballard Nexa 1200 fuel cell module with its monitoring software.
Three metal hydride canisters from Heliocentris with storage capacities of 800 NL hydrogen.

- Power supply from BK Precision.
- Power resistors.
- Programmable DC electronic load from BK Precision.
- MicroLabBox-dSPACE DS1202 with Control Desk®/software® plugged in a Pentium 4 personal computer.
- Semikron IGBT module (SEMITEACH).
- Power card together with measurement card.

- Two ferrite inductance.
- Two hall effect current sensors.
- Two voltage sensors.
- A digital scope.

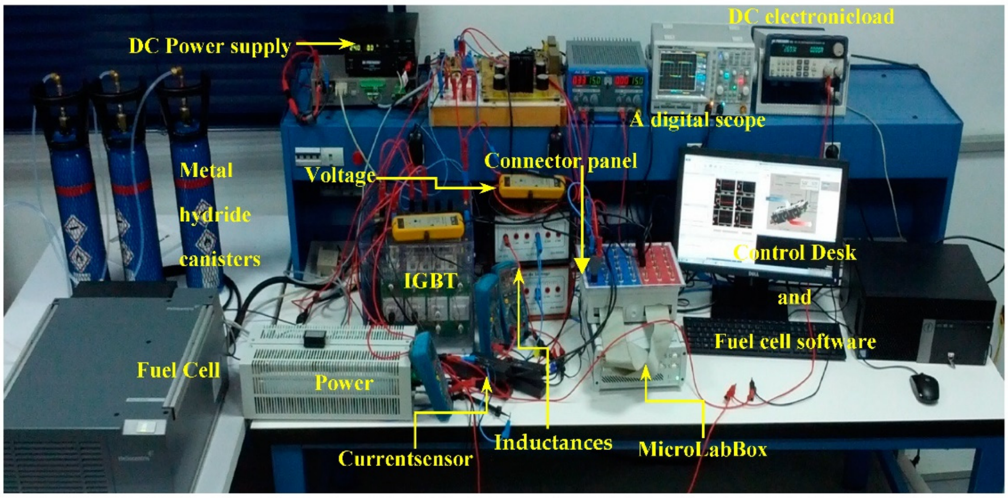

Figure 17. Laboratory prototype used for experimental validation.

The load resistance changes are programmed using the programmable DC electronic load. The controlled system characteristics are summarized in Table 4. The adaptive control design parameters are shown in Table 5. The number of parallel branches of the IBBC is $N = 2$.

Table 4. Controlled system parameters.

	Parameter Designation	Value
Fuel Cell	Ballard Nexa 1200 fuel cell module the fuel cell has a rated power of 1.2 kW	
IBBC	Number of IBBCs	$N = 2$
	Filtering inductance	$L_1 = L_2 = 4$ mH
	Filtering capacitor	$C = 110$ μF
	ESR of the inductance	$r_1 = r_2 = 0.3\ \Omega$
	Switching frequency	$f_s = 20$ kHz

Table 5. The design control parameters.

Parameter	Value
$C_{11} = C_{12}$	2000
C_2	90,000
γ	0.002
η_0	1.077

The load switches from 90 Ω to 30 Ω and returns to 90 Ω. The reference signal of the DC-bus voltage is set to $V_{dc} = 24$ V.

Figure 18 illustrates the voltage measurement of v_{dc} and its reference signal V_d. In this figure, one can observe that the controller behavior is satisfactory. Indeed, the DC-bus v_{dc} perfectly tracks its reference V_d.

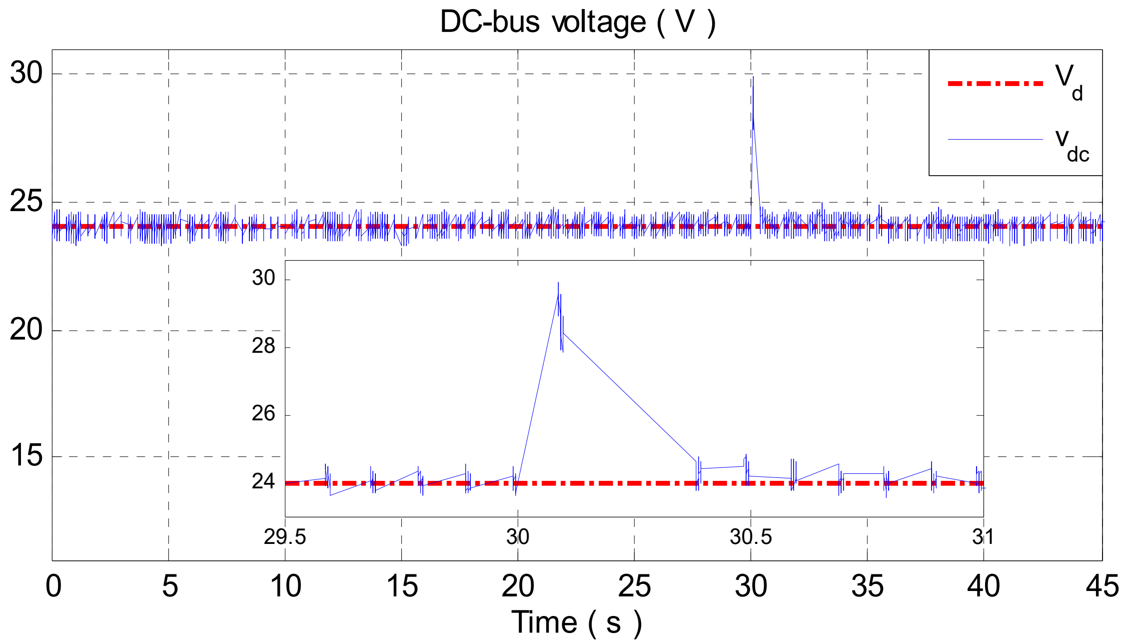

Figure 18. Voltage measurement of v_{dc} and its reference signal V_d.

Figure 19 shows that the inductance currents are equal to the variation in the load. So, the equal current sharing between IBBC branches is ensured. This figure clearly shows that the desired current $I_{\rm d}$ was well estimated.

Figure 20 shows that the online estimate of the unknown parameter θ converges to its true value.

Figure 21 shows the voltage v_{fc} of the fuel cell in the presence of load variations.

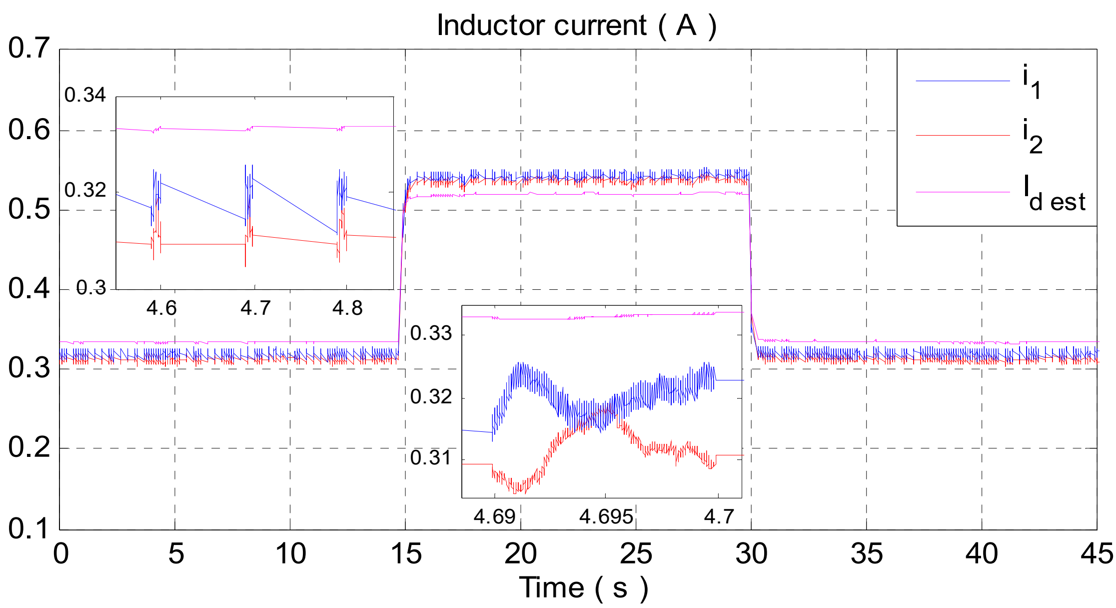

Figure 19. Inductance currents i_k of IBBC and its desired value $I_{d\ est}$.

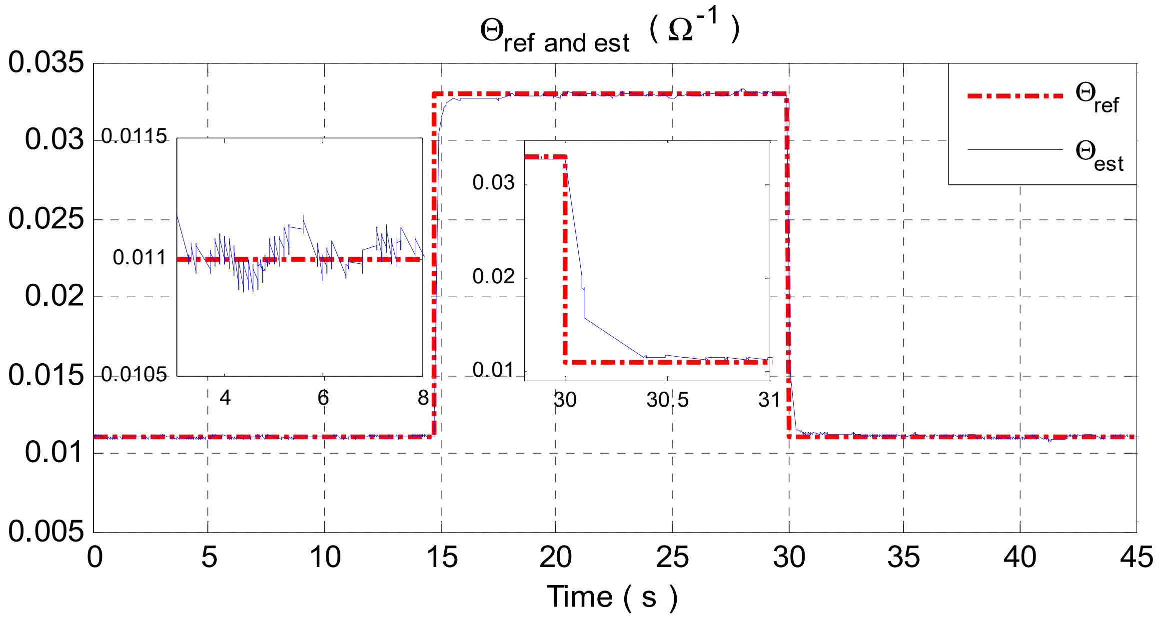

Figure 20. Estimate unknown parameter θ and its reference.

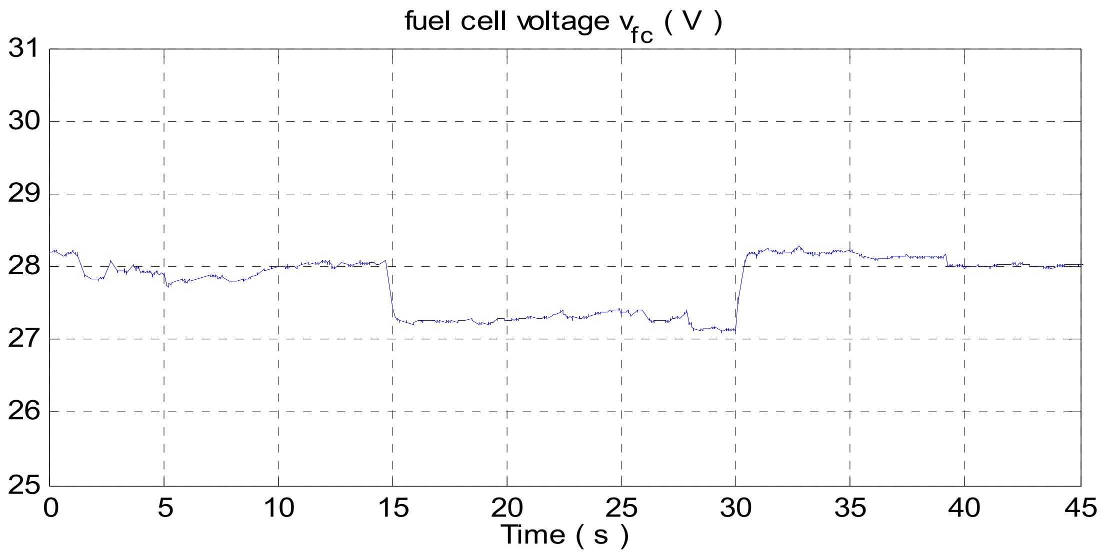

Figure 21. Fuel cell voltage v_{fc}.

Figure 22 illustrates the capacitor voltage v_c.

Figures 23 and 24 show the control signals μ_{1k} and the PWM signals, with a switching frequency of 20 kHz.

The experimental results confirm the performances established in the theoretical analysis and simulation. Specifically, the DC-bus voltage regulation and the equal current sharing between modules are well ensured, etc.

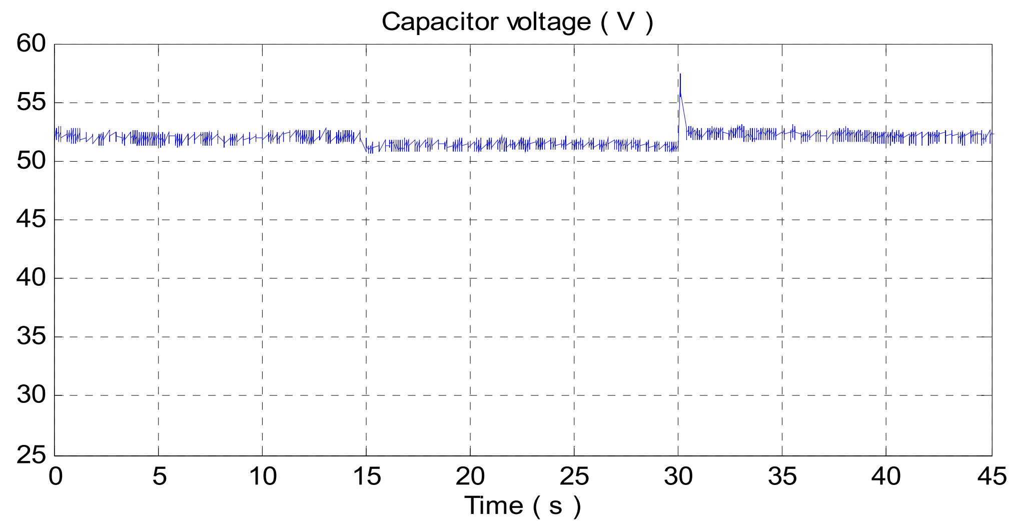

Figure 22. Capacitor voltage v_c.

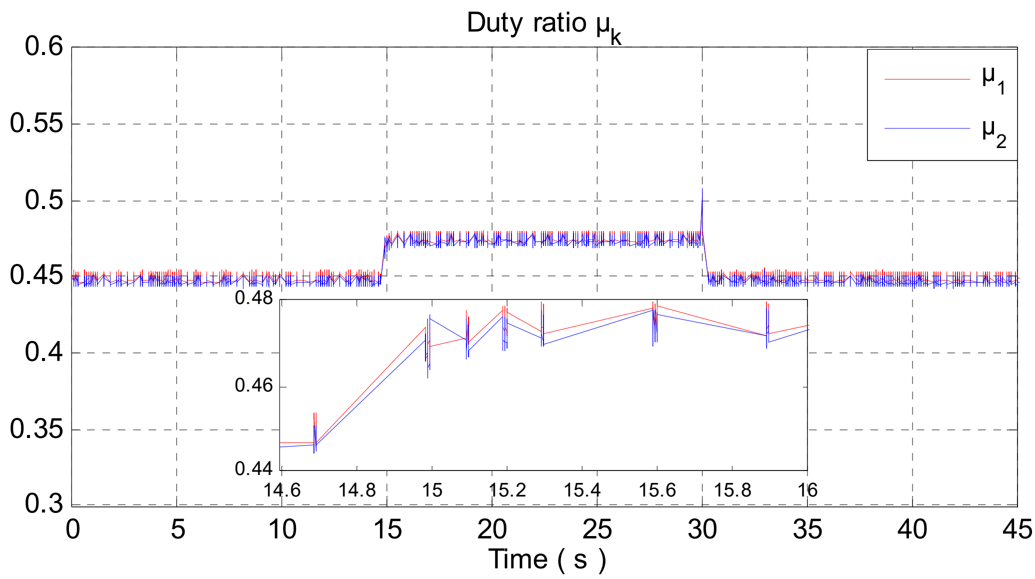

Figure 23. Control signals μ_k with zoom.

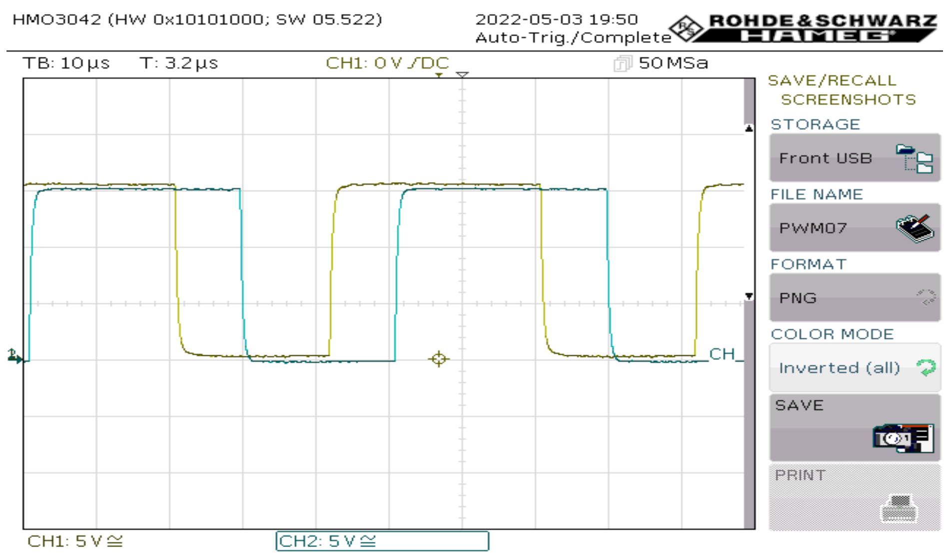

Figure 24. Pulse width modulation of IBBC.

5. Conclusions

The problem of controlling an interleaved Buck–Boost converter connected to a fuel cell energy source is dealt with in this paper. The control objectives are as follows: (i) output DC-bus voltage regulation under load uncertainty (this is necessary to maintain the voltage constant in the DC-bus), (ii) equal current sharing between IBBC branches, especially when supplying heavy loads, and (iii) asymptotic stability of the closed-loop system. To meet these objectives, we have developed an adaptive state-feedback controller that consists of nonlinear control laws. Using theoretical analysis, simulation study, and experimental tests, we have shown that the proposed controller indeed meets all the control objectives.

Author Contributions: Formal analysis, M.K. and H.E.F.; Methodology, H.E.F. and F.G.; Resources, A.R.; Software, Z.E.I., F.Z.B. and K.G.; Supervision, H.E.F. and F.G.; Validation, M.K., Z.E.I. and A.L.; Visualization, F.Z.B. and A.R.; Writing—original draft, M.K., Z.E.I. and K.G.; Writing—review and editing, A.L. and F.G. All authors have read and agreed to the published version of the manuscript.

Funding: This research received no external funding.

Institutional Review Board Statement: Not applicable.

Informed Consent Statement: Not applicable.

Data Availability Statement: Not applicable.

Acknowledgments: The authors gratefully acknowledge the support of the Moroccan Ministry of Higher Education (MESRSFC) and the CNRST under grant number PPR/2015/36.

Conflicts of Interest: The authors declare no conflict of interest.

References

1. Brand, C.; Anable, J.; Ketsopoulou, I.; Watson, J. Road to zero or road to nowhere? Disrupting transport and energy in a zero carbon world. *Energy Policy* **2020**, *139*, 111334. [CrossRef]
2. Chen, H.; Wang, Z.; Xu, S.; Zhao, Y.; Cheng, Q.; Zhang, B. Energy demand, emission reduction and health co-benefits evaluated in transitional China in a 2 °C warming world. *J. Clean. Prod.* **2020**, *264*, 121773. [CrossRef]
3. El Idrissi, Z.; El Fadil, H.; Belhaj, F.Z.; Lassioui, A.; Oulcaid, M.; Gaouzi, K. Theoretical Design and Experimental Validation of a Nonlinear Controller for Energy Storage System Used in HEV. *World Electr. Veh. J.* **2020**, *11*, 49. [CrossRef]
4. Zhang, M.; Fan, X. Review on the State of Charge Estimation Methods for Electric Vehicle Battery. *World Electr. Veh. J.* **2020**, *11*, 23. [CrossRef]
5. Fathabadi, H. Combining a proton exchange membrane fuel cell (PEMFC) stack with a Li-ion battery to supply the power needs of a hybrid electric vehicle. *Renew. Energy* **2019**, *130*, 714–724. [CrossRef]
6. Qi, Z. *Proton Exchange Membrane Fuel Cells*; CRC Press: Boca Raton, FL, USA, 2013.
7. James, L. *Fuel Cell Systems Explained*, 2nd ed.; Wiley: New York, NY, USA, 2003.
8. Abdelfatah, K.; Gaillard, A.; De Bernardinis, A.; Bethoux, O.; Hissel, D.; Khatir, Z. A review on DC/DC converter architectures for power fuel cell applications. *Energy Convers. Manag.* **2015**, *105*, 716–730.
9. VenkateshNaik, M.; Samuel, P. A Non-Inverting Multi Device Interleaved Buck Boost Converter for Fuel Cell Low Voltage Applications. In Proceedings of the 2019 Global Conference for Advancement in Technology (GCAT), Bangaluru, India, 18–20 October 2019; pp. 1–7. [CrossRef]
10. Velázquez-Elizondo, P.E.I.; Araujo-Vargas, A.; Villarruel-Parra, F.J.; Gómez-Olguín, K.; Cano, P.; Granados-Luna, T.R. Six-phase dual-interleaved buck-boost converter for high power-density automotive applications. *J. Eng.* **2019**, *17*, 3592–3597. [CrossRef]
11. Izci, D.; Ekinci, S. A novel improved version of hunger games search algorithm for function optimization and efficient controller design of buck converter system. e-Prime—Advances in Electrical Engineering. *Electron. Energy* **2022**, *2*, 100039. [CrossRef]
12. Rahimi, T.; Islam, M.R.; Gholizadeh, H.; Mahdizadeh, S.; Afjei, E. Design and Implementation of a High Step Up DC-DC Converter Based on the Conventional Boost and Buck-Boost Converters with High Value of the Efficiency Suitable for Renewable Application. *Sustainability* **2021**, *13*, 10699. [CrossRef]
13. Thi Kim Nga, T.; Park, S.-M.; Park, Y.-J.; Park, S.-H.; Kim, S.; Van Cong Thuong, T.; Lee, M.; Hwang, K.C.; Yang, Y.; Lee, K.-Y. A Wide Input Range Buck-Boost DC–DC Converter Using Hysteresis Triple-Mode Control Technique with Peak Efficiency of 94.8% for RF Energy Harvesting Applications. *Energies* **2018**, *11*, 1618. [CrossRef]
14. Azer, P.; Emadi, A. Generalized State Space Average Model for Multi-Phase Interleaved Buck, Boost and Buck-Boost DC-DC Converters: Transient, Steady-State and Switching Dynamics. *IEEE Access* **2020**, *8*, 77735–77745. [CrossRef]
15. Rahimi, T.; Ding, L.; Kheshti, M.; Faraji, R. A ZVS Three-Phase Interleaved DC-DC converter with SFM control method for the Microgrid Applications. In Proceedings of the 2020 11th Power Electronics, Drive Systems, and Technologies Conference (PEDSTC), Tehran, Iran, 4–6 February 2020; pp. 1–5. [CrossRef]

16. Rahimi, T.; Ding, L.; Faraji, R.; Kheshti, M.; Pou, J. Performance Improvement of a Three-Phase Interleaved DC–DC Converter Without Requiring Antisaturation Control for Postfault Conditions. *IEEE Trans. Power Electron.* **2021**, *36*, 7378–7383. [CrossRef]
17. Sampath, S.; Rahiman, Z.; Chenniappan, S.; Sundaram, E.; Subramaniam, U.; Padmanaban, S. Efficient Multi-Phase Converter for E-Mobility. *World Electr. Veh. J.* **2022**, *13*, 67. [CrossRef]
18. Cheddadi, Y.; El Idrissi, Z.; Errahimi, F.; Es-sbai, N. Robust integral sliding mode controller design of a bidirectional DC charger in PV-EV charging station. *Int. J. Digit. Signals Smart Syst.* **2021**, *5*, 137–151. [CrossRef]
19. Elamri, O.; Oukassi, A.; El Bahir, L.; El Idrissi, Z. Combined Vector and Direct Controls Based on Five-Level Inverter for High Performance of IM Drive. *World Electr. Veh. J.* **2022**, *13*, 17. [CrossRef]
20. Gaouzi, K.; El Fadil, H.; Belhaj, F.Z.; El Idrissi, Z. Model predictive control of an inverter for electric vehicles applications. In Proceedings of the 2020 IEEE 2nd International Conference on Electronics, Control, Optimization and Computer Science (ICECOCS), Kenitra, Morocco, 2–3 December 2020. [CrossRef]
21. Belhaj, F.Z.; El Fadil, H.; Idrissi, Z.E.; Koundi, M.; Gaouzi, K. Modeling, Analysis and Experimental Validation of the Fuel Cell Association with DC-DC Power Converters with Robust and Anti-Windup PID Controller Design. *Electronics* **2020**, *9*, 1889. [CrossRef]
22. Wu, X.; Shi, W.; Du, J. Dual-Switch Boost DC–DC Converter for Use in Fuel-Cell-Powered Vehicles. *IEEE Access* **2019**, *7*, 74081–74088. [CrossRef]
23. El Fadil, H.; Giri, F.; Guerrero, J.M.; Tahri, A. Modeling and Nonlinear Control of a Fuel Cell/Supercapacitor Hybrid Energy Storage System for Electric Vehicles. *IEEE Trans. Veh. Technol.* **2014**, *63*, 3011–3018. [CrossRef]
24. Slah, F.; Mansour, A.; Hajer, M.; Faouzi, B. Analysis, modeling and implementation of an interleaved boost DC-DC converter for fuel cell used in electric. *Int. J. Hydrogen Energy* **2017**, *42*, 28852–28864. [CrossRef]
25. Zhang, Y.; Liu, H.; Li, J.; Sumner, M.; Xia, C. DC–DC Boost Converter With a Wide Input Range and High Voltage Gain for Fuel Cell Vehicles. *IEEE Trans. Power Electron.* **2019**, *34*, 4100–4111. [CrossRef]
26. Gao, D.; Jin, Z.; Liu, J.; Ouyang, M. An interleaved step-up/step-down converter for fuel cell vehicle applications. *Int. J. Hydrogen Energy* **2016**, *41*, 22422–22432. [CrossRef]
27. Intidam, A.; El Fadil, H.; El Idrissi, Z.; Lassioui, A.; Rachid, A.; Jabal Laafou, A. Speed Control of a Brushless DC Motor Powered by a PEM Fuel Cell. In Proceedings of the 2021 9th International Renewable and Sustainable Energy Conference (IRSEC), Morocco, 23–27 November 2021; pp. 1–6. [CrossRef]
28. Belhaj, F.Z.; El Fadil, H.; El Idrissi, Z.; Intidam, A.; Koundi, M.; Giri, F. New Equivalent Electrical Model of a Fuel Cell and Comparative Study of Several Existing Models with Experimental Data from the PEMFC Nexa 1200 W. *Micromachines* **2021**, *12*, 1047. [CrossRef] [PubMed]
29. Erickson, R.; Maksimovic, D. Power electronics. In *Fundamentals of Power Electronics*; Springer: New York, NY, USA, 2001.
30. Yu, X.; Starke, M.R.; Tolbert, L.M.; Ozpineci, B. Fuel cell power conditioning for electric power applications: A summary. *IET Electr. Power Appl.* **2007**, *1*, 643–656. [CrossRef]
31. Fontes, G.; Turpin, C.; Astier, S.; Meynard, T.A. Interactionsbetween fuel cells and power converters: Influence of current harmonics on a fuel cell stack. *IEEE Trans Power Electron.* **2007**, *22*, 670e8. [CrossRef]
32. Rosas-Caro, J.C.; Sanchez, V.M.; Vazquez-Bautista, R.F.; Morales-Mendoza, L.J.; Mayo-Maldonado, J.C.; Garcia-Vite, P.M.; Barbosa, R. A novel DC-DC multilevel SEPIC converter for PEMFC systems. *Int. J. Hydrogen Energy* **2016**, *41*, 23401–23408. [CrossRef]
33. Valdez-Resendiz, J.E.; Sanchez, V.M.; Rosas-Caro, J.C.; Mayo-Maldonado, J.C.; Sierra, J.M.; Barbosa, R. Continuous input-current buck-boost DC-DC converter for PEM fuel cell applications. *Int. J. Hydrogen Energy* **2017**, *42*, 30389–30399. [CrossRef]
34. Gerard, M.; Poirot-Crouvezier, J.-P.; Hissel, D.; Pera, M.-C. Ripple current effects on pemfc aging test by experimental and modeling. *ASME J. Fuel Cell Sci. Technol.* **2011**, *8*, 021004. [CrossRef]
35. Chang, C.; Knights, M.A. Interleaving technique in distributed power conversion systems. *IEEE Trans. Circuits Syst. I Fundam. Theory Appl.* **1995**, *42*, 245–251. [CrossRef]
36. Wang, Y.; Wang, C.-Y. Transient Analysis of Polymer Electrolyte Fuel Cells. *Electrochim. Acta* **2005**, *50*, 1307–1315. [CrossRef]
37. Amrouche, F.; Mahmah, B.; Belhamel, M.; Benmoussa, H. Modélisation d'une Pile à Combustible PEMFC Alimentée Directement en Hydrogène-Oxygène et Validation Expérimentale. *Rev. Des Energ. Renouv.* **2005**, *8*, 109–120.
38. Krein, P.T.; Bentsman, J.; Bass, R.M.; Lesieutre, B.L. On the use of averaging for the analysis of power electronic systems. *IEEE Trans. Power Electron.* **1990**, *5*, 182–190. [CrossRef]
39. Goudarzian, A.; Khosravi, A.; Raeisi, H.A. Optimized sliding mode current controller for power converters with non-minimum phase nature. *J. Frankl. Inst.* **2019**, *356*, 8569–8594. [CrossRef]
40. Khalil, H.K. *Nonlinear Systems Analysis*; Prentice Hall Inc.: Upper Saddle River, NJ, USA, 2003.
41. Lee, J.-W. Constructive and discrete versions of the lyapunov's stability theorem and the lasalle's invariance theorem. *Commun. Korean Math. Soc.* **2002**, *17*, 155–163. [CrossRef]